Scripta Materialia 147 (2018) 93–97

Contents lists available at ScienceDirect

Scripta Materialia

journal homepage: www.elsevier.com/locate/scriptamat

Regular article

A special coarsening mechanism for intergranular helium bubbles upon heating: A combined experimental and numerical study

Jie Gao [a,b], Hefei Huang [a,*], Xiang Liu [c], Chengbin Wang [a], James F. Stubbins [c], Yan Li [a,*]

[a] Shanghai Institute of Applied Physics, Chinese Academy of Sciences, Shanghai 201800, China
[b] School of Physical Sciences, University of Chinese Academy of Sciences, Beijing 100049, China
[c] Department of Nuclear, Plasma, and Radiological Engineering, University of Illinois at Urbana-Champaign, Urbana, IL 61801, USA

ARTICLE INFO

Article history:
Received 22 November 2017
Received in revised form 25 December 2017
Accepted 4 January 2018

Keywords:
Intergranular helium bubbles
Coarsening mechanism
In situ TEM heating
Analytical modelling

ABSTRACT

Here, by using *in situ* transmission electron microcopy, we discovered a special mechanism governing the coarsening of intergranular helium bubbles, which exhibit pancake-like growth along grain boundaries to achieve coalescence with another bubble upon heating at 673 K. The developed analytical model, addressing the stress field induced by the bubble internal pressure, well reproduced the observed shape evolution during the bubble growth. Moreover, we show that the coalescing rate of intergranular bubbles was controlled by the surface diffusion and can be accelerated by the pressure gradient between bubbles.

Helium bubbles produced in metals and alloys are typical radiation defects that can lead to swelling, hardening, and embrittlement [1–3]. They tend to aggregate to sinks in metals, especially on grain boundaries (GBs), thus accelerating the failure of polycrystalline materials by reducing the intergranular bonding area *via* bubble coalescence [4–6]. In general, the complex dynamic evolution of helium bubbles in metals would degrade the material performance and even giving rise to a catastrophic failure. Consequently, significant efforts have been made to understand the evolution of helium bubbles under thermal annealing, radiation, or mechanical loading [7–10].

In bubble coarsening upon thermal annealing, two qualitatively different coarsening mechanisms have been distinguished: (i) "Migration and Coalescence" (MC) governed by encounter of migrating bubbles [11–16]. Bubble migration is due to random rearrangements of the bubble surface by diffusion of matrix atoms, most likely by surface diffusion [14]. This kind of coarsening requires bubble motions. (ii) "Ostwald Ripening" (OR) driven by the differences in helium pressure between bubble interiors [11–16]. Because of the thermal activation, helium atoms and/or vacancies were dissociated from small bubbles and reabsorbed by the larger bubbles. It means the small bubbles shrink and even vanish to feed the larger ones. Generally, MC and OR are expected to be dominant at relatively low and high temperature (and/or high and low helium concentrations), respectively [14]. These two mechanisms are concluded mainly from the behaviors of helium bubbles in grain interiors, where the bubbles usually have spherical shapes before and after the thermal annealing. However, the circumstance becomes inherently complex when the bubble coarsening proceeds at GBs [17]. Experimental studies using *in situ* TEM have shown that irradiation-induced intergranular helium bubbles can perform a Brownian-type motion along general GBs at heating temperature of 793 K and 833 K (>0.8 T_m where T_m is the absolute melting temperature) in pure aluminum [18,19]. Although the bubble coalescence was observed, it fails to capture the important intermediate dynamical process due to the fast movement of bubbles. This limits our basic understanding of the coarsening kinetics of intergranular helium bubbles, which play a key role in clarifying the nature of the failure of helium-irradiated metals and the basic properties of inert gases in solids.

In this study, by conducting *in situ* heating experiments at an appropriate temperature inside a transmission electron microscope, we observed the whole dynamical process of the growth and coalescence of nanoscale intergranular helium bubbles because of the decelerated bubble movement. A well-annealed polycrystalline nickel foil (99.95 wt%) was firstly irradiated by 1.2 MeV helium ions to the fluence of 6.75×10^{16} ions/cm^2 at room temperature and subsequently to the same fluence of 4.50×10^{16} ions/cm^2 by the following energies 1.1, 1.0, 0.9, 0.8, 0.7, 0.6 and 0.5 MeV. Before the irradiation, a piece of nickel foil with the thickness of 950 nm was mounted in front of the actual sample as an energy degrader. The purpose for using muli-energy helium irradiation and energy degrader were to achieve a relatively uniform helium distribution within the sample. The ion beam intensity was kept ~1 μA during the irradiation process. The cross-sectional TEM sample, used in the *in situ* heating experiment, was prepared using a focused ion beam (FIB, FEI Nanolab 600). An observation spot, including three

* Corresponding authors.
E-mail addresses: huanghefei@sinap.ac.cn (H. Huang), liyan@sinap.ac.cn (Y. Li).

https://doi.org/10.1016/j.scriptamat.2018.01.006
1359-6462/

GBs that were conjugating at a tripe node, was chosen at a depth of ~596 nm from the irradiated surface. Fig. 1(a) schematically shows the EBSD scan of these three adjacent grains. The misorientation angles between the neighboring grains were 37.1°, 19.3° and 47.9° with corresponding rotation axes of $[42\bar{1}]$, $[\bar{2}21]$ and $[\bar{2}01]$, respectively. The misorientation data were calculated using TexTools, a texture analysis software package. At these GBs, helium bubbles with a nominal diameter of ~5 nm are formed as shown in Fig. 1(b). Obviously, these bubbles are much larger than those formed besides them in the grain interiors. Since the Fig. 1(b) was obtained at a low magnification before the heating, the GBs cannot be seen clearly. Further observation at high magnification during the heating can evidence that the larger nanoscale helium bubbles are actually on the GBs. It is clear that these intergranular bubbles have spherical shapes before the heating was applied.

Bubbles perform deformation and thus to achieve coalescence at GBs evidence that a special mechanism, differing from the previous MC and OR mechanisms, has governed the bubble coarsening kinetics. On the one hand, OR mechanism occurs because of the dissociation of helium atoms and/or vacancies from bubbles [14]. Obviously, this process was hard to be activated at 673 K in nickel. Therefore, OR mechanism for bubble coarsening were inhibited in this study. On the other hand, MC mechanism needs bubble movement (mainly the Brownian motion) [14,18,19], here the bubbles kept their central positions unchanged before the coalescence. Perhaps, the Brownian motion of helium bubbles along general GBs requires high activation energy and it did not triggered by the heating at 673 K (~0.4 T_m) in nickel. However, the behavior that bubble contact together and then coalesce was much similar with bubble behavior controlled by MC mechanism. Therefore, the governing mechanism can be identified as a special MC mechanism for bubble growth at GBs.

Actually, the MC and OR mechanisms are experimentally concluded mainly from the coarsening behaviors of helium bubbles that locate in isotropic environment of grain interiors. The non-isotropic environment of planar grain boundaries where helium bubbles grow in this study is believed to result in the arising of this special mechanism. Presumably, the nickel self-diffusion along the grain boundary plane has participated in the growth of intergranular bubbles and even played an important role.

The growth kinetics of intergranular helium bubbles can be described by two main processes: (i) The matrix atoms flow along the bubble-matrix interface to the triple junction, and (ii) The matrix atoms from the interface enter and flow along the grain boundary [22]. In this study, we developed an analytical model based on a finite difference numerical scheme to follow the bubble evolution during the heating process (See ***supplementary material***). Fig. 3(a) shows the calculated three-dimensional evolution of a typical intergranular helium bubble. It is clear that the bubble radius, *R1* and *R3*, on the GB plane enlarges, whereas the radius *R2* normal to the GB plane shrinks as the heating proceeds. The corresponding projective shapes (Fig. 3(b)) continuously alter from the disc shape to ones elongated along the GB, agreeing well with the observed bubble behavior in the heating experiment. To quantify the bubble deformation, we defined a parameter f as $f = R1/R2$. The lower panel in Fig. 3(c) shows that the parameter f increases monotonously from 1 (initial spherical bubble) to a constant value of 2.1 (final elongated bubble). The constant f reveals a final stable shape of the evolving bubble. This deduction is confirmed by the elongated bubbles that keep unchanged in shape as shown in Fig. 2(c, d, e), except *B1* and *B2* because of their coalescence. In fact, the analytical model predicts the existence of a steady state when the normal stress σ_n acting on the grain boundary balances the traditional capillary stress $\sigma_{cap} = \gamma_s \cdot (\kappa_1 + \kappa_2)$ at the bubble tip. The apparent f of the three stable bubbles near *B1,2* in Fig. 2(e) was measured to be ~1.9. Repeated measurements were performed to reduce the error in the estimation of the two radii due to the somewhat blurry TEM micrograph. Note that the GB plane between the Grains I and Grain II (Fig. 1(a)) has an inclination of ~31.8° with respect to the direction of incident electrons (See ***supplementary material***). Therefore, their real f are slightly higher than 1.9, which indicates the actual final deformation of bubbles will be in better coincidence as compared with results ($f = 2.1$) obtained in the analytical model.

As expected, the pressure P within the bubble is shown to decrease due to the increasing bubble volume during the heating (upper panel in Fig. 3(c)). The stress σ_n, however, is shown to increase at the incipient stage of bubble growth. The reason is that the proportion of internal pressure P, acting on bubble-matrix interface, increased in the direction normal to the GB when the bubble evolves from spherical to elongated. The increase in stress σ_n induced by the bubble elongation is larger than the decrease caused by the pressure drop before the heating time of ~654 s where f is less than ~1.5. As the pressure further drops, stress σ_n decreases until it balances the traditional capillary stress σ_{cap} at the bubble tip. In the final stage, the upper panel in Fig. 3(c) shows that the pressure P and thus induced stress σ_n still drops. The cause is that the surfaces between the tip and the top of bubble were adjusting their positions because of the local curvature gradients when the bubble tip was reaching thermodynamic equilibrium. Based on the relations that controls the bubble evolution (see ***supplementary material***) and the parameter of heating time (2179.6 s) for the formation of stable bubbles, the surface diffusivity D_s of nickel atoms has been estimated to be quite low as 6.9×10^{-22} m^2/s at 673 K in the analytical model.

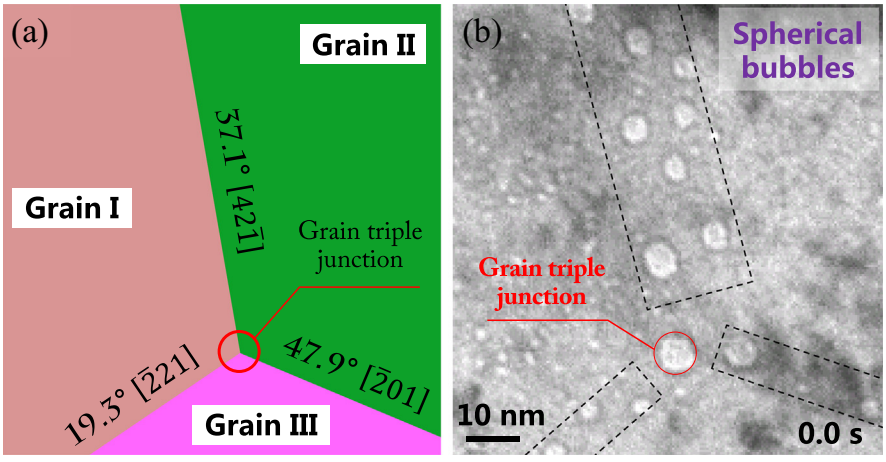

Fig. 1. Geometry of grain boundaries and distribution of intergranular helium bubbles. (**a**) Schematic EBSD scan shows the three adjoined grains. (**b**) Underfocus image of helium bubbles along GBs and in nearby grain interiors right before the heating (0.0 s). The dash line rectangles indicate the GBs between the neighboring grains.